# ERROR ANALYSIS IN THE JOINT EVENT LOCATION/SEISMIC CALIBRATION INVERSE PROBLEM

William L. Rodi

Massachusetts Institute of Technology

Sponsored by Air Force Research Laboratory

Contract No. F19628-03-C-0109

## ABSTRACT

The goal of this project is to develop new mathematical and computational techniques for analyzing the uncertainty in seismic event locations, as induced by both observational errors and errors in the travel-time model used in the location process. The analysis is being done in the context of the multiple-event inverse problem, in which the locations of multiple events are inferred jointly with travel-time corrections for the event-station paths. The premise is that one of the events is the target of the location uncertainty analysis while the others are calibration events that serve to constrain the path corrections within some level of error. Performing uncertainty analysis on the coupled location/calibration inverse problem takes implicit account of how errors in the inferred path corrections affect the location of the target event and, conversely, how errors in the calibration event locations affect the path corrections.

To date, the project has addressed the case in which travel-time corrections are parameterized as a simple time term for each station/phase combination in the data set. Under this assumption, the first year's effort resulted in a scheme for computing a confidence region on the target event location, in a fully nonlinear sense, that reflects the total uncertainty in all of the parameters of the joint location/calibration problem. These "multiple-event" confidence regions are computed with a two-step procedure: (1) generating a map of the likelihood function on a grid encompassing the best fitting location of the target event, and (2) performing a Monte Carlo simulation to determine a confidence level for each value of likelihood in the map. Each step requires repeated solution of the multiple-event inverse problem, making the method very computationally intensive. A major focus of the project has been to speed up the method, which was achieved last year by simplifying the second step (Monte Carlo simulation) and has been addressed in the current year by designing better grids for the first step (likelihood mapping) and by making the underlying grid-search single-event location algorithm that both steps use more efficient. Additional accomplishments of the current year were (1) a technique for computing multiple-event confidence regions that are based on the traditional Gaussian/linear assumptions, which provide a useful baseline for evaluating the fully nonlinear confidence regions, and (2) incorporating the ability to apply "soft" constraints on location parameters and travel-time corrections in the form of prior probability distributions, as an alternative to the hard constraints used previously. This paper illustrates these new capabilities using data from the Nevada Test Site.

## OBJECTIVE

The objective of this project is to develop new mathematical and computational techniques for quantifying the errors in seismic event locations, including the effects of observational errors and errors in the travel-time forward model. Our approach associates the latter, or *model errors*, with the uncertainty in path travel-time corrections that have been inferred from calibration data. We thus analyze event location uncertainty in the context of the joint location/calibration inverse problem, whereby arrival time data from multiple events and stations are used to simultaneously locate the events and estimate calibration parameters that underlie the travel-time corrections. One of the multiple events is taken to be a new event under investigation while the remaining events are calibration events. Calibration parameters can be, for example, explicit travel-time corrections for paths, travel-time correction surfaces, or a 3D velocity model that generates travel-time corrections via ray tracing. A complete error analysis that considers the errors in all the unknown parameters—the location of the new event, the locations of non-GT0 calibration events, and the calibration parameters—accounts for the key sources of error in the new event location, including picking errors in the observed arrival times for the new *and* calibration events, and errors in the calibration event locations.

We are addressing this joint inverse problem with numerical techniques, like grid search and Monte-Carlo simulation, that lift key limitations of analytic approaches to uncertainty analysis in large inverse problems. These limitations include the restriction to Gaussian data errors, the necessity of using a linear approximation to the travel-time forward model, and restricted mechanisms for incorporating *a priori* constraints on the unknowns (notably, Gaussian prior distributions). Moreover, analytic approaches typically provide only Gaussian descriptions of location uncertainty, such as variance matrices and confidence ellipses, which may inadequately characterize uncertainty when Gaussian/linear assumptions are violated.

## RESEARCH ACCOMPLISHED

### Summary of Approach

Rodi (2004) presented the mathematical formulation of the joint location/calibration inverse problem and maximum-likelihood uncertainty approach that are the basis for this project. To summarize, we write the joint inverse problem as

$$d_{ij} = T_j(\mathbf{x}_i) + t_i + c_{ij} + e_{ij} \qquad (1)$$

where $i$ indexes each of $m$ seismic events and $j$ indexes each of $n$ station/phase combinations that have been observed from one or more of the events. Then, $d_{ij}$ denotes the arrival time observation for the $i$th event and $j$th station/phase (($i$,$j$)th path); $\mathbf{x}_i$ and $t_i$ are the origin parameters (hypocenter and time, respectively) of the $i$th event; $T_j$ is a model-based travel-time function for the $j$th station/phase; $c_{ij}$ is a correction to this function for path ($i$,$j$); and $e_{ij}$ is an observational error. This equation holds only for the paths ($i$,$j$) for which data have been observed. The unknown parameters of the joint location/calibration inverse problem are the event hypocenters and origin times, $\mathbf{x}_i$, $t_i$, $i = 1,\ldots,m$, and the path travel-time corrections, $c_{ij}$. The joint location/calibration problem is often referred to as the *multiple-event location* problem.

To date, this project has focused on the "basic" multiple-event location problem, in which the path corrections are assumed to be event-independent (see Jordan and Sverdrup, 1981; Pavlis and Booker, 1983):

$$c_{ij} = a_j. \qquad (2)$$

The calibration parameters then comprise a time term, $a_j$, for each station/phase pair in the data set. Other ways of parameterizing path corrections include reciprocal correction functions (Rodi et al., 2003) and velocity models, and these will be addressed later in the project.

Our approach to uncertainty analysis is based on likelihood functions, which quantify how well any given values for the parameters agree with the observed data. The likelihood function is determined by the assumed probability

distribution of the observational (picking) errors in the data, $e_{ij}$. We have assumed that these errors are statistically independent and that each has a *generalized Gaussian* probability distribution of order $p$ (Billings et al., 1994). For basic multiple-event location, this error model implies a likelihood function, $L$, given by

$$-\log L = \mathbf{const} + \sum_{ij} \log \sigma_{ij} + \frac{1}{p} \sum_{ij} \frac{1}{(\sigma_{ij})^p} \left| d_{ij} - T_j(\mathbf{x}_i) - t_i - a_j \right|^p . \quad (3)$$

In this paper we will assume the data standard errors, $\sigma_{ij}$, are known *a priori*. The task of maximizing $L$ with respect to the event location and calibration parameters is equivalent to minimizing an $l_p$ norm (to the $p$th power) of the data residuals, as given by the last term of equation (3). The case of Gaussian errors coincides with $p = 2$.

In previous projects we have developed an algorithm called GMEL (grid-search multiple-event location) for maximizing the likelihood function in equation (3). GMEL solves jointly for the location parameters of the events, $\mathbf{x}_i$ and $t_i$, and the travel-time correction terms of the station/phase combinations, $a_j$. It accepts prior constraints on all the parameters in the form of upper and lower bounds on each unknown parameter (e.g. $a_j^{\min} \le a_j \le a_j^{\max}$) . Bounds on an event epicenter take the form of a maximum epicentral distance from a specified geographic point. The algorithm used by GMEL is described in Rodi et al. (2002).

**Location confidence regions**

Our approach to uncertainty analysis in the joint location/calibration (multiple-event location) inverse problem extends the formulation of Rodi and Toksöz (2001) for the single-event location problem, i.e. the special case in which there is one event ($m = 1$) and the path corrections ($c_{1j}$) are assumed known. We can summarize the approach for both problems as follows. Let the vector **p** contain the subset of unknown problem parameters on which a confidence region is desired, and let the vector **q** contain the remaining "hidden" parameters. For example, **p** may be the hypocenter of the first event, i.e. $\mathbf{p} = \mathbf{x}_1$. In single-event location, **q** would then be simply the origin time of the event: $\mathbf{q} = (t_1)$. In the multiple-event location problem, however, **q** contains $t_1$, all the other event locations and the travel-time corrections:

$$\mathbf{q} = (t_1, \mathbf{x}_2, t_2, \ldots, \mathbf{x}_m, t_m, a_1, a_2, \ldots, a_n). \quad (4)$$

To address the uncertainty in the *epicenter* of event 1, as another example, we would move its depth, $z_1$, from **p** to **q**. Let **d** denote the vector of relevant arrival time observations: the $d_{ij}$ in the multiple-event problem, or $d_{1j}$ in the single-event problem. We can write the likelihood function for both problems as $L(\mathbf{p},\mathbf{q};\mathbf{d})$.

A confidence region on **p** is defined in terms of a test statistic, $\tau(\mathbf{p},\mathbf{d})$, which compares the likelihoods that are achieved with **p** fixed to a particular value and with **p** free to vary (within prior bounds). In each case **q** is free to vary within its bounds. Let us define the (negative) log-likelihood function relevant to **p** as

$$\Lambda(\mathbf{p},\mathbf{d}) = -\log \max_{\mathbf{q}} L(\mathbf{p},\mathbf{q};\mathbf{d}). \quad (5)$$

The test statistic is then defined as

$$\tau(\mathbf{p},\mathbf{d}) = \Lambda(\mathbf{p};\mathbf{d}) - \min_{\mathbf{p}'} \Lambda(\mathbf{p}';\mathbf{d}) \equiv \Lambda(\mathbf{p},\mathbf{d}) - \Lambda(\mathbf{p}^*;\mathbf{d}) \quad (6)$$

where **p*** is the maximum-likelihood solution for **p**. A confidence region on **p** at confidence level β (e.g. β =90 %) is the locus of points satisfying

$$\tau(\mathbf{p}, \mathbf{d}) \le \tau_\beta \quad (7)$$

where $\tau_\beta$ is a critical value of the probability distribution of $\tau(\mathbf{p},\mathbf{d})$, as induced by the errors in **d**.

**Confidence region algorithm**

This project is developing a numerical algorithm for computing multiple-event confidence regions appropriate for Gaussian or non-Gaussian errors and accounting for the nonlinearity of the forward travel-time model and the effects of nonlinear parameter constraints (e.g. hard bounds). The algorithm is a two-step procedure:

1. *Likelihood mapping*: $\Lambda(\mathbf{p};\mathbf{d})$ is evaluated on a dense grid in **p**-space, centered on **p***. For example, the likelihood map is a function of the epicenter of event 1 when an epicenter confidence region is sought.

2. *Monte Carlo simulation*: $\tau(\mathbf{p}^*,\mathbf{d}^{syn})$ is evaluated for many realizations of synthetic data, $\mathbf{d}^{syn}$.

The likelihood map from Step 1 is converted to a map of $\tau(\mathbf{p},\mathbf{d})$, using equation (6). The results of Step 2 are used to estimate the critical statistic $\tau_\beta$. The results of both steps can then be combined into a map of the confidence region, as defined in (7). Rodi (2004) and Rodi and Toksöz (2001) describe these two steps in more detail.

Both steps of this procedure entail maximizing the likelihood function with respect to **q**, or both **p** and **q**, many times. In multiple-event location, each maximization entails solving for multiple event locations and travel-time corrections, resulting in a very computationally intensive algorithm. Our early implementations of the procedure required up to one hour of CPU time, on a 2.4 Ghz Xeon processor, to perform each step for *epicenter* confidence regions on the Nevada Test Site (NTS) events discussed below. Rodi (2004) discussed how Step 2 (Monte Carlo simulation) is sped up tremendously (less than 1 minute of CPU time) with the use of a reasonable approximation; namely, that $\tau_\beta$ does not depend on the constraints applied to **q**. The speed-up of Step 2 is thus achieved by holding the calibration event locations fixed. This cannot be done in Step 1, however.

In the current year, we have made several improvements to our location uncertainty approach. These include further increases in algorithm speed, achieved by improving the underlying single-event grid-search algorithm used by GMEL, and by using more efficient grids in Step 1 of the multiple-event confidence region algorithm. More significantly, we have developed some new capabilities that provide a means for evaluating our uncertainty results. The next sections describe and demonstrate these new capabilities.

**Quadratic Approximations**

Expanding the log-likelihood function, $\Lambda$ in equation (5), in a second order Taylor series around the maximum-likelihood solution, **p***, provides a quadratic approximation to this function. Denoting the approximation as $\Lambda_2$ (and hiding the explicit dependence on **d**) we have

$$\Lambda_2(\mathbf{p}) = \Lambda(\mathbf{p}^*) + \mathbf{g}(\mathbf{p}^*)^T(\mathbf{p}-\mathbf{p}^*) + \frac{1}{2}(\mathbf{p}-\mathbf{p}^*)^T\mathbf{H}(\mathbf{p}^*)(\mathbf{p}-\mathbf{p}^*) \tag{8}$$

where $\mathbf{g}(\mathbf{p}^*)$ denotes the gradient vector of $\Lambda$ with respect to **p**, and $\mathbf{H}(\mathbf{p}^*)$ denotes the Hessian matrix of $\Lambda$, both evaluated at $\mathbf{p} = \mathbf{p}^*$. The gradient and Hessian exist for any exponent of the error distribution greater than 1, $p > 1$, as long as the travel-time forward functions, $T_j(\mathbf{x})$, have finite first and second derivatives. Additionally, if each component of **p*** lies between its prior bounds, we have $\mathbf{g}(\mathbf{p}^*) = 0$. Referring to equation (6), the test statistic resulting from the quadratic approximation to $\Lambda$ then becomes

$$\tau_2(\mathbf{p}) = \frac{1}{2}(\mathbf{p}-\mathbf{p}^*)^T\mathbf{H}(\mathbf{p}^*)(\mathbf{p}-\mathbf{p}^*) \tag{9}$$

When the data errors are Gaussian ($p = 2$) and if second derivatives of the travel-time functions can be ignored, the approximation is exact: $\Lambda_2 = \Lambda$ and $\tau_2 = \tau$. Moreover, the probability distribution of $\tau_2$ is known analytically, i.e., $2\tau_2$ is chi-squared distributed with $k$ degrees of freedom, where $k$ is the number of target parameters (dimensionality of **p**). Under these circumstances, a confidence region on **p** is the ellipsoid given by

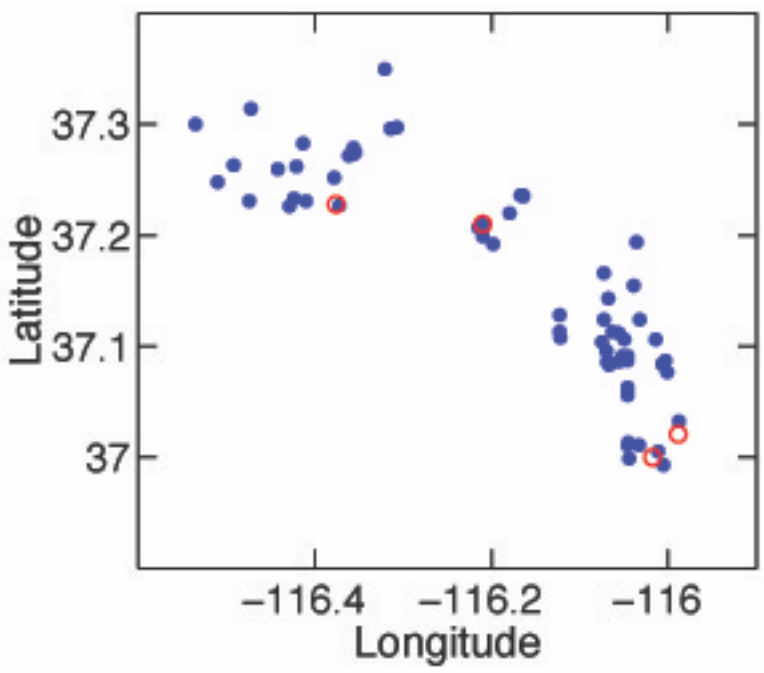


**Figure 1. GT0 locations of 71 NTS explosions used for testing our uncertainty algorithm. The event shown as a red circle near 37.2°N, 116.2°W is a well-recorded explosion at Rainier Mesa that was constrained as a GT event in our tests. The other three red circles are a Pahute Mesa explosion and two Yucca Flat explosions for which multiple-event confidence regions were computed.**

$$\left(\mathbf{p}-\mathbf{p}^*\right)^T \mathbf{H}\left(\mathbf{p}-\mathbf{p}^*\right) \le \chi_k^2(\beta) \tag{10}$$

where the right-hand side is the critical value of the chi-squared distribution for the confidence level β. (This result was first obtained by Evernden, 1969). In this case, the confidence region is concisely described by the ellipsoid axis lengths and orientations, which are easily obtained from the eigenvalue decomposition of **H**.

Event location algorithms typically calculate the confidence ellipsoids of equation (10) by constructing the Hessian analytically from the first derivatives of the travel-time forward functions, ignoring second derivatives and thus nonlinearity of the forward problem. When computing single-event confidence regions, GMEL computes ellipse parameters for epicenters using this same technique. The technique could also be applied to multiple-event confidence regions, but the Hessian calculation becomes much more difficult. This is because analytic computation of the Hessian with respect to **p** requires the computation, and inversion, of the full Hessian with respect to **p** and the hidden parameters **q**. In single-event location there are few hidden parameters (e.g. just origin time) but in multiple-event location there are many, as indicated in equation (4).

Therefore, we have developed a numerical technique for computing the Hessian of Λ with respect to **p**. The technique entails sampling Λ at a small number of points in *p*-space near **p***, and then approximating **H** with finite second differences of the sample values. Computing Λ at each grid point requires maximizing the likelihood with respect to the hidden parameters, i.e. solving a multiple-event location problem. The computations are thus like those done in Step 1 of our general confidence region algorithm. However, only a few grid points are involved instead of the dense grid required to map Λ.

While ellipsoidal, multiple-event confidence regions derived from the quadratic approximation are only exact for Gaussian errors and when nonlinearity is negligible, GMEL computes them in all situations to provide a comparison to the more general confidence regions obtained with our two-step algorithm described above.

**Examples with Nevada Test Site data**

We are testing our new uncertainty analysis techniques on regional seismic arrival times from Nevada Test Site explosions, for which precise locations and origin times are known. The data set was generated by Lawrence Livermore National Laboratory (LLNL) (see Walter et al., 2003). To date, our tests have used only a subset of the Pn arrivals, obtained by removing two stations (TPH and DAC) that are within 1.5° of most of the explosions, as well as events with fewer than 4 arrivals and stations with fewer than 2 arrivals. The resulting subset comprises 548 Pn picks from 71 events and 38 stations. Figure 1 shows the GT0 locations of the 71 events.

Confidence regions were computed for three of the events having relatively few arrivals: an event from the Pahute Mesa testing area and two from Yucca Flat. These events are shown as red circles in Figure 1. When considering each of these three events in turn, the remaining 70 events were treated as calibration events. Only one of the calibration events, however, was assigned a finite GT accuracy: a well-recorded Pahute Mesa explosion (20 Pn arrivals), which is also shown as a red dot in Figure 1. The GT level of this event was varied in the experiments: GT0, GT2 or GT5. The 69 other calibration events help to constrain the unknown travel-time corrections ($a_j$) even though no prior information on their locations is used. The corrections themselves were assigned hard bounds of ±5 sec, which is effectively unconstrained. All event depths were fixed to their true values in these tests. Furthermore, the origin times of the events, including the ground-truth calibration event, were unconstrained. The tests were done with the IASP91 travel-time tables as the forward model. Picking errors were assumed to be Gaussian with a standard deviation of 0.325 sec.

Figure 2 compares single-event and multiple-event confidence regions for the three target events. The single-event regions (left panels) are smaller because they assume that the path travel-time corrections are known exactly (zero). In multiple-event location, in contrast, the corrections are estimated jointly with the event locations. The multiple-event confidence regions (right panels) account for the additional location uncertainty induced by uncertainty in the estimated corrections. The multiple-event confidence regions in Figure 2 assume the ground-truth event at Rainier Mesa is GT0. Therefore, the multiple-event confidence regions do not account for any location uncertainty for the GT event.

The ellipse plotted on each panel of Figure 2 is the 90% confidence ellipse computed under the quadratic approximation, using the new likelihood differencing technique described above. We see that, for both the single-event and multiple-event cases, the ellipses match the numerically computed 90% confidence regions (blue areas) quite closely. This indicates, first of all, that in these cases the effects of nonlinearity are small. Secondly, it indicates that our differencing method for calculating the Gaussian/linear confidence ellipses is accurate. For the single-event case, in fact, the ellipses derived from the likelihood-differenced Hessian matrix are virtually identical to those derived from the analytically computed Hessian (the traditional approach; see Flinn, 1965).

Figure 3 compares multiple-event confidence regions for the same three target events, obtained with different assumptions about the location accuracy of the GT calibration event at Rainier Mesa. The left panels are the same as the right panels in Figure 2 (GT0 case). The center panels assume the GT event is GT2, while the right ones assume it is GT5. We see that, as expected, the confidence regions become larger as the assumed accuracy of the GT event location worsens. We also see that the Gaussian/linear 90% confidence ellipses (black circles) depart increasingly from the numerically computed 90% regions (blue areas) as the GT accuracy degrades. This implies that the effects of nonlinearity become more important as the location error increases.

We note that the GT2 and GT5 cases in Figure 3 used a hard constraint on the GT calibration event. In the GT2 case, for example, the GT event location was constrained to be within a 2 km radius of the known (GT0) location of the event. The next section compares this to the use of soft bounds on locations.

**Soft Constraints on Locations and Corrections**

In the current year, we also enhanced GMEL to allow "soft" constraints on parameters as an alternative to hard bounds. The soft constraint on a given parameter takes the form of a prior probability distribution, which multiplies the likelihood function implied by the arrival data (as in Bayesian inference methods). We take the prior

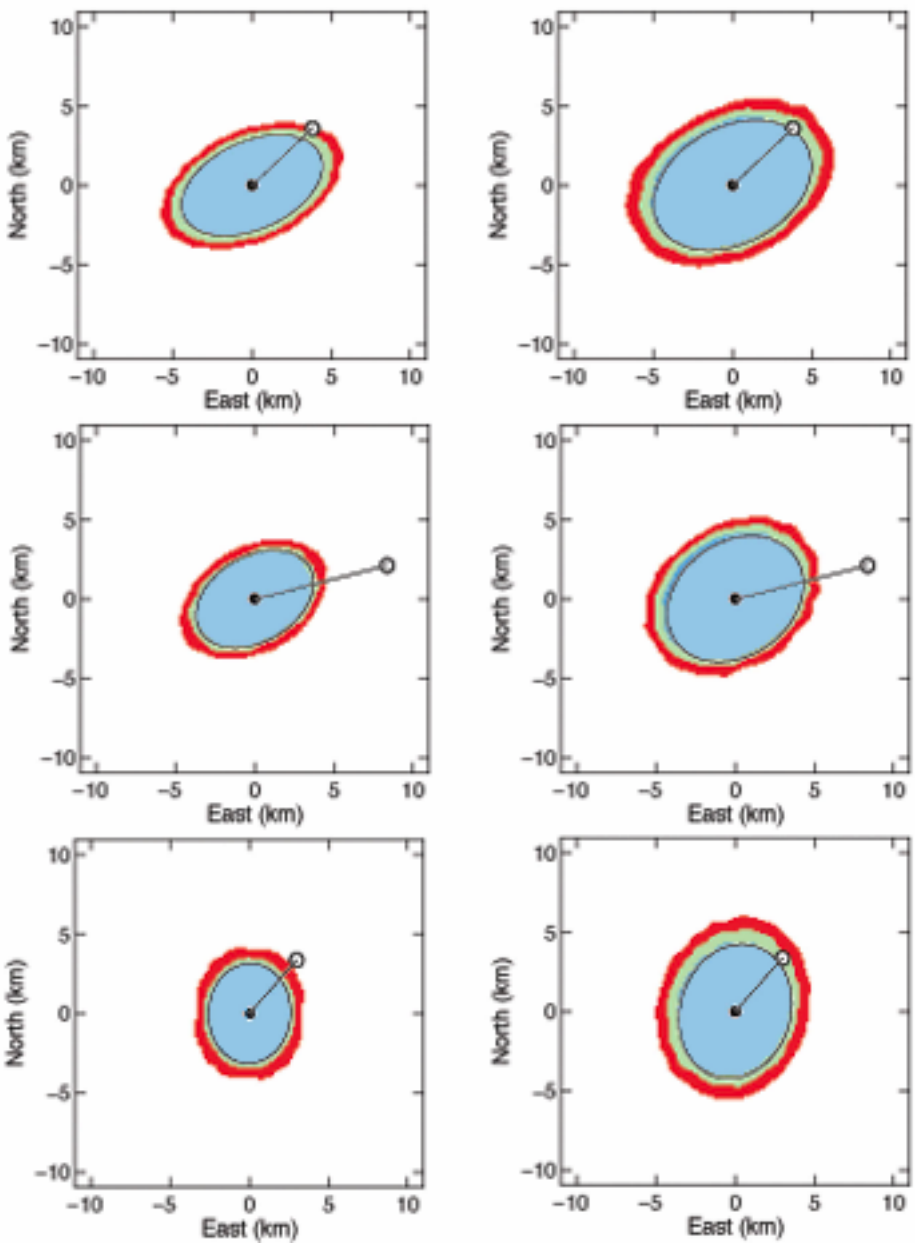


**Figure 2. Epicenter confidence regions for three NTS events. *Top:* a Pahute Mesa explosion with 6 Pn arrivals. *Center:* a Yucca Flat explosion with 7 Pn arrivals. *Bottom:* a Yucca Flat explosion with 8 Pn arrivals. The frames on the left show *single*-event confidence regions (path travel-time corrections assumed known). The frames on the right show *multiple*-event confidence regions (path corrections unknown), computed with one well-recorded Rainier Mesa explosion constrained to be a GT0 event. Confidence regions are shown for 90, 95 and 98% confidence (blue, green and red, respectively). In each frame the black circle marks the maximum-likelihood solution for the event and the white circle is its GT0 location (from Walter et al., 2003). The ellipse in each frame is the 90% confidence ellipse determined under the Gaussian/linear approximation.**

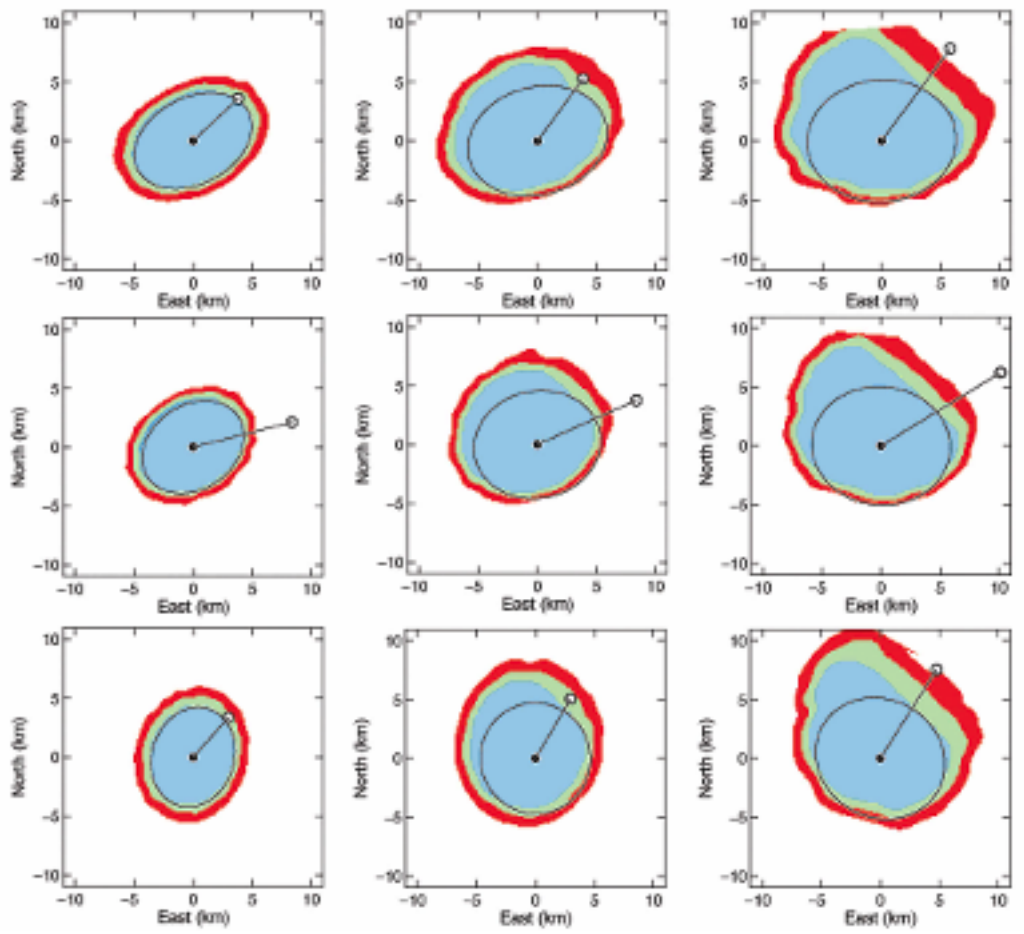


**Figure 3. Multiple-event confidence regions for three NTS events (one at Pahute Mesa, two at Yucca Flat) computed with different GT levels for the ground-truth event at Rainier Mesa: GT0 (left), GT2 (center) and GT5 (right). The events are ordered from top to bottom the same way as in Figure 2, and plotting conventions are the same as in that figure.**

distributions on parameters to be of the generalized Gaussian type, as we assume for the data errors. Thus, for example, a soft constraint on a travel-time correction, $a_j$, adds a term to the log-likelihood function of the form

$$\Lambda\left(a_j; a_j^0\right) = \frac{1}{p(\sigma_j)^p}\left|a_j - a_j^0\right|^p . \tag{11}$$

The constraint is thus specified with a parameter prior mean $\left(a_j^0\right)$, standard error ($\sigma_j$) and order of the generalized Gaussian ($p$). The epicentral latitude ($\theta_i$) and longitude ($\phi_i$) of an event are constrained jointly by adding the prior log-likelihood given by

$$\Lambda\left(\theta_i, \phi_i; \theta_i^0, \phi_i^0\right) = \frac{1}{p(\sigma_i)^p}\left[X\left(\theta_i, \phi_i; \theta_i^0, \phi_i^0\right)\right]^p \tag{12}$$

where $X$ denotes the epicentral distance function.

As now implemented, each type of parameter can have a different distribution order $p$, which in turn can be different from that assigned to the data errors. When $p = 2$, the prior distribution on a parameter is Gaussian. As $p$ increases, the distribution becomes "boxier", and the parameter constraint approaches the use of hard bounds.

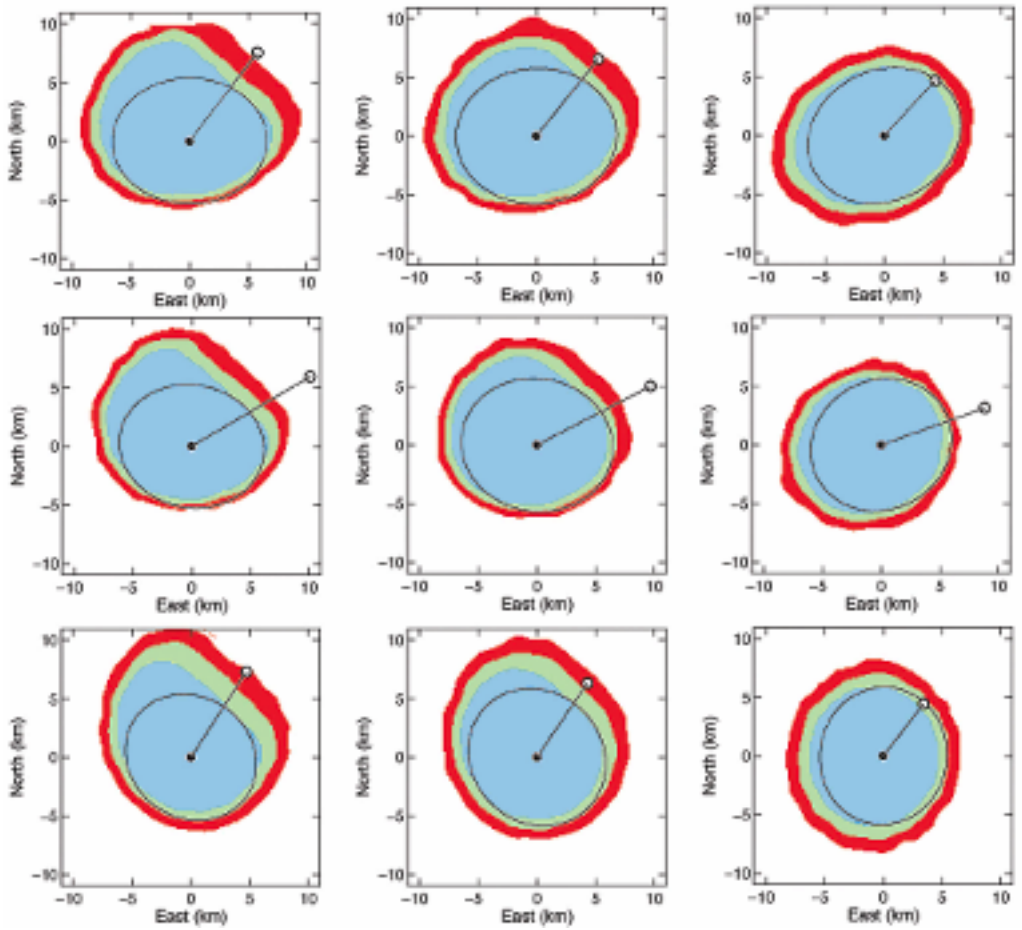


**Figure 4. Multiple-event confidence regions for the three NTS events, computed using soft constraints on the location of the GT event. Three values of the order of the prior distribution are compared: $p = 20$ (left), $p = 5$ (center) and $p = 2$ (right). In each case, the prior distribution corresponded to a GT5 constraint at 90% confidence. Plotting conventions are the same as in Figures 2 and 3.**

**Examples with Nevada Test Site data**

Figure 4 shows multiple-event confidence regions for the three target events we have been considering, computed using soft, instead of hard, GT constraints on the well-recorded Rainier Mesa event. Three values of the prior distribution order $p$ in equation (12) were used: 20 (left frames), 5 (center) and 2 (right), corresponding to three levels of "hardness" of the GT location constraint. All the results in Figure 4 took the GT event to be GT5, which means that the 5 km circle surrounding the prior location contains 90% of the prior probability distribution.

The confidence regions in the left column of Figure 4 look similar to the right column of Figure 3 because $p = 20$ generates a very boxy prior distribution and the GT constraint is essentially a hard GT5 bound. As the constraint is softened (center and right columns), we see that the numerical confidence become more elliptical. For $p = 2$, they are not very different from the Gaussian/linear approximations. We can thus identify the non-ellipticity of confidence regions seen in the examples of this paper mainly with the use of hard constraints on GT event locations.

## CONCLUSIONS AND RECOMMENDATIONS

We have made significant progress in the development of numerical techniques for event location uncertainty analysis in the framework of the joint location/calibration inverse problem, which considers the effects of both picking and model errors on event location errors. The techniques compute "multiple-event" confidence regions without need of the convectional assumptions of Gaussian errors and linearity of the forward problem. An important

accomplishment of the current year, ironically, was the development of a simple, efficient technique for computing multiple-event confidence regions *under* the Gaussian/linear assumption, for these provide the opportunity to evaluate our more general approach. The numerical experiments performed thus far, using data from the Nevada Test Site, indicate that Gaussian/linear confidence ellipses are an adequate description of the errors in event *epicenters* when Gaussian probability distributions are used for both the observational error model and prior constraints on event locations. The implication is that nonlinearity of the travel-time forward model does not invalidate the approximation. It remains to be seen whether this holds for hypocentral confidence regions and focal depth confidence intervals, which we have discovered to be quite susceptible to travel-time nonlinearity in the single-event location problem.

While we made good progress on improving the computational efficiency of our general uncertainty method, it is not yet clear whether it will be a practical tool for routine analysis, especially when more complex parameterizations of travel-time corrections are considered (e.g., correction surfaces). If not, the method will still be a valuable laboratory instrument for studying the limitations of approximate confidence regions. We point out that our technique for computing elliptical approximations to location confidence regions is quite efficient and, since it involves similar computations as the more general method (sampling the likelihood function on a grid), it is possible that a hybrid of the two techniques could be a practical approach to routine nonlinear, non-Gaussian analysis of event location uncertainty.

## ACKNOWLEDGMENTS

I wish to thank Steve Myers of LLNL, who provided the NTS explosion data set.

## REFERENCES

Billings, S.D., M.S. Sambridge and B.L.N. Kennett (1994), Errors in hypocenter location: picking, model and magnitude dependence, *Bull. Seism. Soc. Am., 84*, 1978-1990.

Evernden, J.F. (1969), Precision of epicenters obtained by small numbers of world-wide stations, *Bull. Seism. Soc. Am.* 59: 1365-1398.

Flinn, E.A. (1965), Confidence regions and error determinations for seismic event location, *Rev. Geophys.* 3*:* 157-185.

Jordan, T.H. and K.A. Sverdrup (1981), Teleseismic location techniques and their application to earthquake clusters in the south-central Pacific, *Bull. Seism. Soc. Am., 71*,1105-1130.

Pavlis, G.L, and J.R. Booker (1983), Progressive multiple event location (PMEL), *Bull. Seism. Soc. Am.* 73: 1753-1777.

Rodi, W. (2004), Error analysis in the joint event location/seismic calibration inverse problem, in *Proceedings of the 26th Seismic Research Review, Trends in Nuclear Explosion Monitoring*, LA-UR-04-5801, Vol. 1, pp. 307-316.

Rodi, W. and M.N. Toksöz (2001), Uncertainty analysis in seismic event location, in *Proceedings of the 23rd Seismic Research Review*, *Worldwide Monitoring of Nuclear Explosions,* LA-UR-01-4454, Vol. 1, pp. 324-332.

Rodi, W., E. R. Engdahl, E. A. Bergman, F. Waldhauser, G. L. Pavlis, H. Israelsson, J. W. Dewey and M.N. Toksöz (2002), A new grid-search multiple-event location algorithm and a comparison of methods, in *Proceedings of the 24th Seismic Research Review—Nuclear Explosion Monitoring: Innovation and Integration,* LA-UR-02-5048, Vol. 1, pp. 403-411.

Rodi, W., S.C. Myers and C.A. Schultz (2003), Grid-search location methods for ground-truth collection from local and regional seismic networks, *Proceedings of the 25th Seismic Research Review—Nuclear Explosion Monitoring: Building the Knowledge Base*, LA-UR-03-6029, Vol. 1, pp. 311-319.

Walter, W.R., K.D. Smith, J. L. O'Boyle, T.F. Hauk, F. Ryall, S.D. Ruppert, S.C. Myers, M. Anderson, and D.A. Dodge (2003), Improving the fundamental understanding of regional seismic signal processing with a unique western United States dataset, in *Proceedings of the 25th Seismic Research Review—Nuclear Explosion Monitoring: Building the Knowledge Base,* LA-UR-03-6029, Vol. 1, pp. 486-494.